PHYSICS AND CHEMISTRY OF SOLID STATE
V. 26, No. 2 (2025) pp. 322-328
Section: Physics

DOI: 10.15330/pcss.26.2.322-328

Vasyl Stefanyk Precarpathian National University

ФІЗИКА І ХІМІЯ ТВЕРДОГО ТІЛА
Т. 26, № 2 (2025) С. 322-328
Фізико-математичні науки

PACS: 78.67.Sc

ISSN 1729-4428 (Print)
ISSN 2309-8589 (Online)

V. Shanmugam[1], P. Manimaran[2], T. Seethalakshmi[1]

Specific capacitance characteristic of Cu nanoparticles embedded in rGO nanosheets using co-precipitation approach

[1]*PG & Research Department of Physics, Government Arts college (Autonomous), Karur, Affiliated to Bharathidasan University, Tiruchirappalli. Tamil Nadu, India, nvsgacphy@gmail.com, seethabala@gmail.com;*
[2]*PG & Research Department of Chemistry, Government Arts college (Autonomous), Karur, Affiliated to Bharathidasan University, Tiruchirappalli, Tamil Nadu, India*

The co - precipitation approach was used to construct reduced graphene oxide (RGO) – supported Cu nanoparticles. PXRD, EDX, and TEM examination validated the crystalline size and functional groups as well as morphological behaviour of these nanoparticles. The powder XRD findings of rGO and Cu-rGO nanocomposites are used to estimate grain size, dislocation density, and micro strain. Cu-rGO nanoparticles are opaque in the optical and near infrared domains, with a reduced cut-off wavelength of 233 nm, according to UV-Visible absorption spectra. The band gap strengths (Eg) of rGO and Cu-rGO nanocomposites were found to be 1.5 and 2.31 eV, correspondingly. Cu-rGO d-spacing values from XRD and Cu-rGO d-spacing values from the SEAD pattern were quite similar. In multi scan rate, the specific capacitance values of rGO and Cu-rGO estimated from CV increased, as did the specific capacitance value.

Keywords: rGO rGO, chemical reduction, Cu/rGO composite, Cyclic voltagramme.

Received 08 April 2024; Accepted 29 April 2025.

Introduction

Graphene oxide (GO) and reduced graphene oxide (rGO) have become a popular trend these days, and they've built creates a completely new sector in material research [1]. For flexible electronics, renewable energy, biomedical, and environmental cleanup, the prospect of integrating graphene with inorganic nanoparticles to generate graphene-nanoparticle hybrid constructions is now extensively addressed [2–4]. The ability of these graphene-nanoparticle hybrid structures for drug and gene delivery is greatly enhanced by behaviours and outcomes and usually beneficial features. Electron transport function in graphene is seen to be impacted by the decorating of metal or metal oxide nanoparticles on graphene substrates, for example, by modifying the localized electronic properties [5-7].

GO, unlike RGO, has a number of functional groups that limit its conductivity. RGO, on the other hand, contains a higher percentage of SP^2 carbon atoms and a lower fraction of oxygen-containing functional groups, enhancing its conductivity. rGO is highly conductive, despite the fact that GO is an insulator, however conductivity varies depending on the degree of reduction. Substantially lower rGO, like pure graphene, is practically a superconductor [8]. Wide-bandgap (WBG) semiconductor materials can be employed in power conversion applications due to their wide band gap, which leads to enhanced energy and temperature behavior, as well as the creation of more intense particles. In comparison to other conducting polymers, reduced graphene oxide (rGO) has a lower energy gap, which inhibits its usage in elevated transistors [9]. By embedding graphite in concentrated acid and exposing it to an oxidising agent, graphene oxide (GO) is created. The Tour approach proved to be less harmful and more successful for graphite oxidation. For graphite oxidation, this procedure, as well as its updated variations, is currently the most extensively utilised [10]. In the most dynamic instances, hydrazine or hydrazine hydrate were used to reduce GO chemically. Conversely, because they have the

ability to be hazardous and damaging [11], caution should be exercised when utilising large doses. As a result, researchers required to look into novel ways for efficiently converting graphene oxide (GO) to reduced graphene oxide (rGO) under mild circumstances [12,13]. The co-precipitation methodology was used in this study to construct copper embedded reduced graphene oxide nanocomposites. PXRD, FTIR, TEM with SAED patterns, EDX spectroscopy, and electrochemical activity recognition assessment also were described.

I. Material Methods

1.1. Chemicals and Instruments

Cupper Chloride ($CuCl_2$), Potassium permanganate ($KMnO_4$), Sodium Borohydride ($NaBH_4$), Sodium hydroxide (NaOH) and H_2O_2 was purchased from Sigma-Aldrich. Sulphuric acid (H_2SO_4), HCl, and EtOH were obtained from AnalaR grade. Without further purification, all chemicals and reagents were used as supplied.

1.2. Preparation of GO and RGO oxide

The graphene oxide were prepared by graphite flakes of about 3g of dissolved 75 ml of H_2S0_4 (98%) volumetric flask. It is kept under at ice bath (0-5°C) with constant stirring at 2 hrs at 0-5°C temperature and potassium permanganate (7g) was added very slowly. The rate of addition was carefully prohibited to keep the reaction temperature lesser than 15°C. The ice bath was removed, and the mixture was stirred at 35°C.The paste became brownish in color and kept under stirring for 2 days. An above the combination is dissolved in 100 ml of water. The reaction temperature was increased to 98°C. The color of the mixture was change into brown. Then the solution was diluted by adding a 200 ml of water and it was stirred continuously. Finally 15 ml of H_2O_2 is added to the solution, yellow color appears in the solution. After that the solution was washed with HCl and Deionized water (DI) by means of rinsing and centrifugation. The Graphene oxide (GO) was obtained as a powder after filtering and drying under vacuum at the room temperature.50mg of GO was dispersed in 50ml of demonized water. 5ml of sodium borohydride was added. Then, this process is treated under ultra-sonication for 2-3 hours. After wards the solution was washed 3 times with ethanol solution and dried in a vacuum at 50^0C for 24 hours. Thus, the dried mixture of an r-GO sheet was collected.

1.3. Synthesis of Cu/r-GO Nano-composite

0.05 g of prepared r-GO by a modified hummer's method was dispersed in 50 ml of water. 0.4753g of $CuCl_2$, 19g $NaBH_4$ and 0.5g NaOH (1Mm) pellets are slowly added to the above same solution. The mixed solution stirred 6 hrs continually. The final products were collected washed with distilled water and ethanol for several times under ultrasonic condition and then dried in a vacuum oven at 45^0C for 8 hrs.

1.4. Characterization of nanocomposites

FTIR spectra were carried out by using Agilent spectrometer. FTIR spectrophotometer in the wavelength range of 4000-400cm^{-1} with the operated resolution of 4cm^{-1} followed by KBr pellet made techniques to deduce the functional groups of the Nanocomposites. The surface morphology of the synthesized nanocmposites were determined using Transmission Electron Microscopy (TEM) on ZEISS and JEM (JEOL-electronic microscopy japan instrument and elemental analysis was carried out by EDX instruments. The structural and crystallite phase were characterized by XRD (powder x-ray diffraction) model (PW3050/60) using CuKα1=1.540 A^0, Kα2 1.544 A^0 (XPERT-PRO software).

II. Results and discussions

2.1. PXRD analysis

The synthesized rGO and Cu-rGO nano particles were characterized by powder x-ray diffraction XRD shows that Figure 1, Cu-Kα radiation. The rGO peak 2θ value is 26.58°(002) is present of hexagonal structure. (reference code: 98-000-7181). The Cu-rGO peaks at 2θ value of 18.49° (011), 26.26° (002), 32.43° (112), 39.31° (022), 50.48° (123) and 53.11° (004) were consistent with the standard XRD data for the Cu-rGO Cubic phase of FCC lattice given in Table 1. These results are demonstrated that r-GO was successfully synthesized and $CuCl_2$ was oxidized to Cu during redox reactions [14].

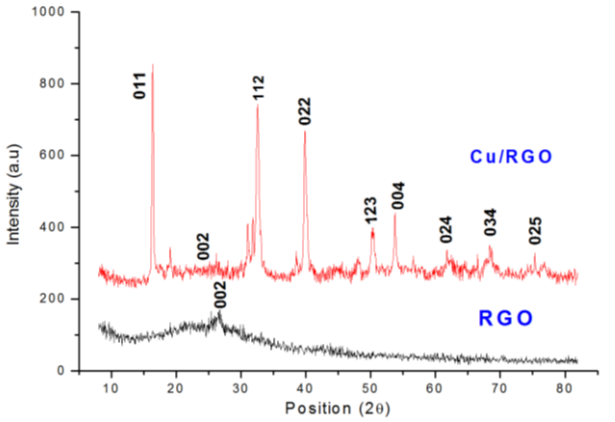

Fig.1. Powder XRD Pattern of (a) r-GO (b) Cu/r-GO.

According to the interpretation provided by the XRD patterning, the graphene oxide arrangement is indicated by the peak position of the 2theta value 16.38°, which corresponds to the d-spacing value at 5.41Å. A reduction in GO is attributed to the values of 19.10° and 4.6 Å. The d-spacing values for 39.98°, 48.20°, and 68° are 2.8 Å, 1.89Å, and 1.38Å, respectively. In extremely crystalline domains, the values mentioned are closely matched with the Cu planes.

Microstrain [%] reflects irregularities in the crystal or lattice distortion. The expansion indicated by positive strain (e.g., 0.5774%) may be the result of the integration of Cu nanoparticles into rGO layers. Compression or stress inside the lattice may be indicated by negative numbers, such as -0.165 %.

Dislocation Density results indicate at lower angles (16°–32°), reduced dislocation concentrations (~10^{-6} $Å^{-2}$) suggest established crystalline areas. Greater dislocation density at greater angles (44°–50°),

Table 1.

XRD spectrum of Cu-rGO (d-spacing)

Pos. [°2Th.]	Height [cts]	FWHM Left [°2Th.]	d-spacing [Å]	Rel. Int. [%]	Dislocation Density δ [Å⁻²]
16.3665	605.32	0.1968	5.41618	100.00	6.01×10^{-6}
19.1140	78.24	0.2952	4.64341	12.92	1.34×10^{-5}
31.0204	158.83	0.1968	2.88298	26.24	5.69×10^{-6}
31.8430	175.85	0.1476	2.81036	29.05	3.19×10^{-6}
32.4914	433.68	0.3444	2.75574	71.64	1.73×10^{-5}
38.5775	59.23	0.2952	2.33385	9.78	1.23×10^{-5}
39.8443	422.78	0.2460	2.26252	69.84	8.48×10^{-6}
44.7421	26.84	1.5744	2.02557	4.43	3.36×10^{-4}
48.0524	49.53	0.7872	1.89347	8.18	8.19×10^{-5}
50.2899	124.13	0.5904	1.81435	20.51	4.53×10^{-5}

particularly at 44.74°, indicate that those planes are more distorted or defective. These numbers align with the tendency for defect concentration to increase with decreasing crystallite size in common nanocrystalline materials.

2.2. Fourier Transforms Infra-Red Spectroscopy

FTIR analysis evaluated that the chemical functionalities present in rGO, Cu/r-GO nanocomposites as shown in figure 2. The FTIR spectrum of r-GO a broad peak between 3000-3700cm^{-1} in the high frequency area together with a sharp peak at 2375 cm^{-1} corresponding to the medium and stretching vibration of N-H group of primary secondary amines and amides molecules adsorbed on rGO of broad peak in range of 2700-3500cm^{-1} in the high frequency. The Cu-rGO nanocomposite of sharp peak at 3488cm^{-1} corresponding to the stretch of H-bonded vibration of OH groups of water molecules adsorbed on Cu-rGO.

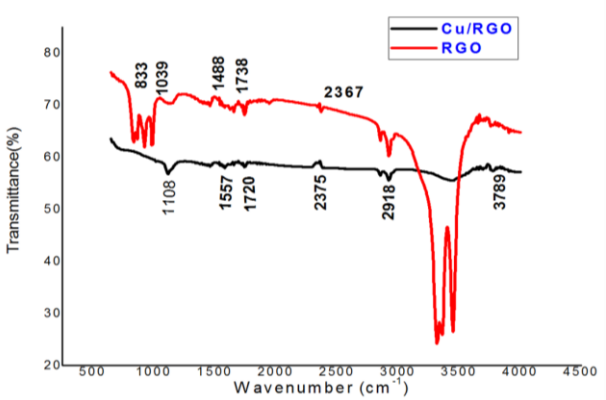

Fig. 2. FT-IR Spectrum of rGO and Cu-rGO nanocomposite.

It is possible to achieve a high degree of hydrophilicity in the sample. The adsorption of rGO and Cu-rGO peaks at 1488-1557cm^{-1} are represent the stretching weak medium and multiple vibrations of C=C bend, while the presence of two absorption peaks observed in the medium frequency area, at 1720cm^{-1} - 1738cm^{-1} it can be attributed to the stretch strong lower wavelength vibration of C=O groups present at the amines, amides. Finally the absorption peaks at 2376cm^{-1} - 2367cm^{-1} are corresponding to the medium stretching vibration of C=C of carbonyl, respectively. The presence of these carbonyl groups reveals that the symmetrical alkynes. The functional groups especially OH result in the formation of hydrogen bonds between Cu-rGO of water molecules. This further explains the hydrophilicity nature of Cu-rGO nanocomposite [15].

2.3. TEM with EDAX analysis

The TEM image analyses show that the Cu NPs prepared using co-precipitation method are significantly smaller in size than the CuNPs on rGO. Figure 3&4 it shows that TEM images of synthesized Cu-rGO nanoparticles. It clear evidence that the rGO nanosheet are present over the Cu nanoparticles. The d-spacing value of Cu-rGO nanoparticles 5.14 nm. From XRD studies that d-spacing values are strongly or matched with d-spacing value Cu-rGO from TEM studies (0.21nm) are given Table 2 [16]. From SAED pattern (112) planes are confirmed Cu nanoparticles are cubic structure. The EDAX spectrum reveals that presence of function on Cu-rGO Shows that Figure 5 point out C, O, Cu and Cl element [17]. In this EDAX spectrum some of the impurities of Cl atoms presented and Cu, O, C atoms have a high intensity peaks are represented in Cu atom embedded on rGO sheet in the rage of 0 to 10 KeV. The compositions of element percentages are indicated on Table 3.

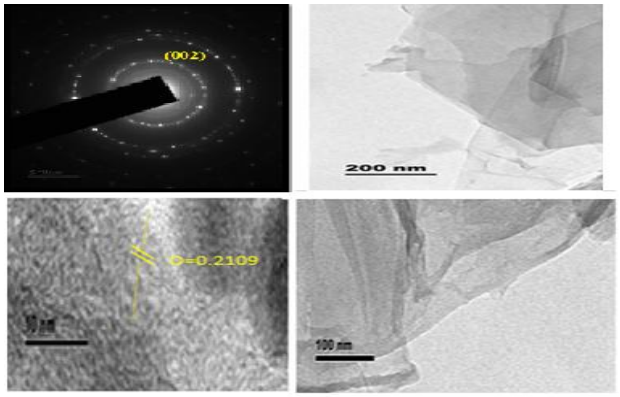

Fig. 3 TEM images, SAED and Diffraction pattern of rGO.

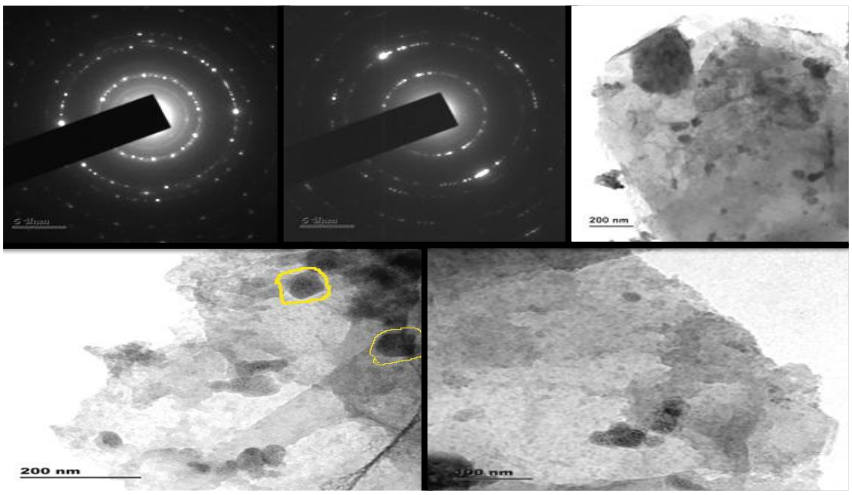

Fig. 4. TEM images, SAED and Diffraction pattern of Cu/r-GO.

Table 2.

TEM image of Cu-rGO d-spacing size

Pos. [°2Th.]	Area [cts*°2Th.]	d-spacing [Å]	Crystallite Size [Å]	Micro Strain [%]	FWHM Left [°2Th.]
16.386(3)	61.7397	5.41886	696.9022	0.4048	0.22(1)
19.10(2)	5.4441	4.65372	538.205	-0.165	0.15(8)
31.09(1)	16.1013	2.88177	334.231	-0.0981	0.22(6)
31.90(2)	11.3335	2.81023	-1249.828	0.2661	0.2(1)
32.62(1)	118.920	2.7497	156.3875	0.3225	0.5(2)
39.977(6)	83.6201	2.25903	223.3423	0.2844	0.44(3)
48.20(6)	7.6009	1.89115	-1328.389	0.5504	1(1)
50.41(2)	24.5901	1.81316	-1338.726	0.5774	0.6(2)
68(3)	130.005	1.3827	-1419.543	0.8559	1(4)

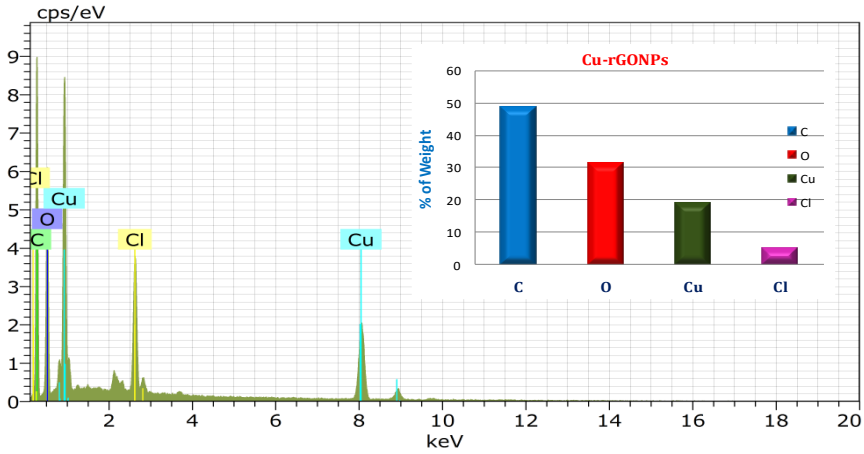

Fig. 5. EDX IMAGE OF (A) rGO, (B) Cu-rGO.

Table 3.

EDX spectrum of (A) rGO, (B) Cu-rGO quantitative results

Element Line	Weight %	Weight % Error	Atom %
C	6k-series	48.67	46.80
O	8k-series	31.14	29.95
Cu	29k-series	19.02	18.29
Cl	17k-series	5.16	4.96
Total	k-series	104.00	100.00

2.4. Optical Studies: UV-Visible Spectroscopy

Optical absorption is a useful instrument for determining the optical energy band gap of crystalline and amorphous materials. The fundamental absorption corresponding to the electron exhibition from the valance band to the conduction band can be used to determine the nature and value of the optical band gap. In previously reported that the Cu Optical band gap energy (2.09) eV and Urbach energy (1.82) eV. From 2.7 eV to 1.15 eV, the optical band gap of rGO can be easily reduced and tuned. In order to determine the optical energy band gap of Cu-

rGO nanoparticles the UV-Vis absorption spectrum was recorded at 200 to 800 nm in figure 6 [18]. The sample shows a strong absorption peak (λmax) at 233 nm attributed to σ to σ* transition in the UV region. The absorption peak at UV region, were used to study the shifting in the optical energy band gap for rGO and Cu-rGO nanocomposite. The energy band gap in optical energy gap is derived from the relationship.

$$(\lambda h\gamma) = B\left(h\gamma - E_g\right)^n$$

Where $h\gamma$ is the photon energy, B is the constant and n is the power factor and that takes 1/2,2,3/2 allowed direct, allowed indirect, forbidden direct and forbidden indirect transitions respectively.

The Fig 6 shows that rGO and Cu-rGO optical band gap value is increase from the value of (1.5) eV to (2.31) eV, which is smaller to the observed for Cu-rGO nanocomposite [19].

2.5. Cyclic voltammetry (CV) study

Cylic voltammetric studies of Cu-rGO nanoparticles were carried out at the scan rate of 2mV/s and as shown in Figure 7. The Ip values varied linearly with the square root of a scan rate as in study, and the peak separation became greater as the scan rate increased. These results reflect and electrochemical behaviour is controlled by the transfer.

The calculated Sp. capacitance values for Cu-rGO nanoparticles were scan rate 1 m/V, 2 m/V, 3 m/V, 4 m/V, 5 m/V, 6 m/V and 7 m/V and their specific capacitance values are 68.37, 83.04, 84.54, 112.22, 116.38, 121,41 and 137.35 F/g, respectively in table 4. This voltammetric

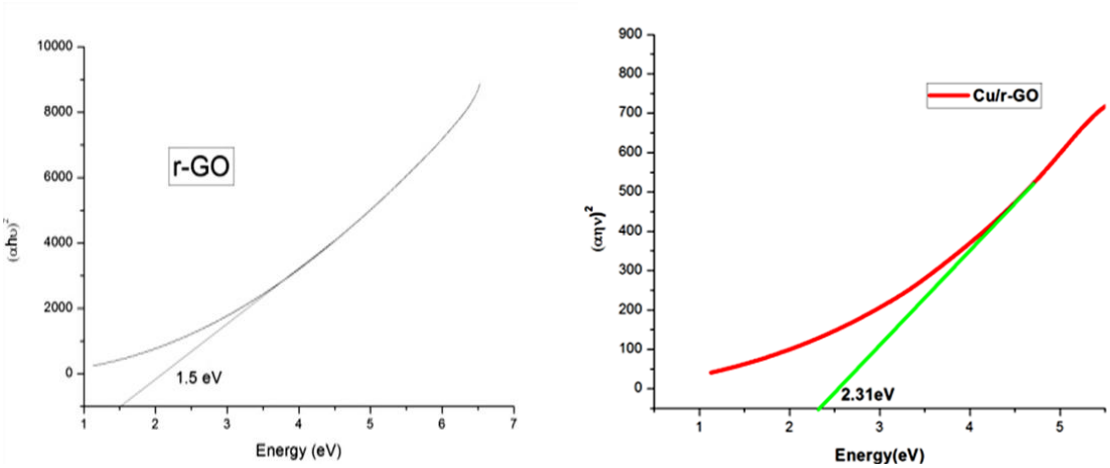

Fig. 6. UV-Visible spectrum of transmittance rGO and Cu-rGO.

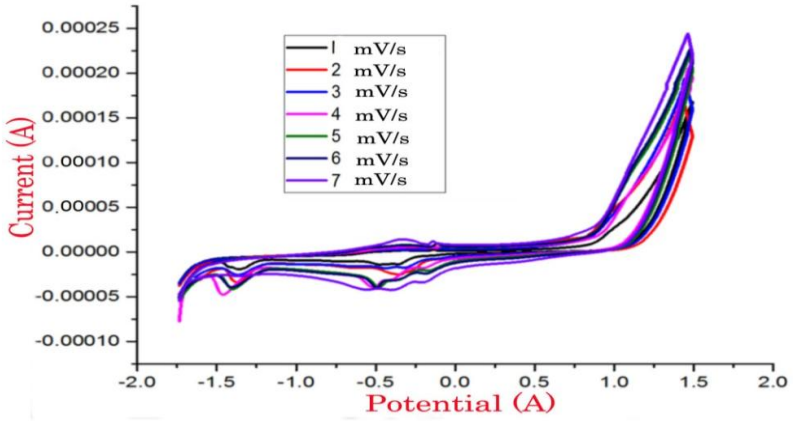

Fig. 7. CV of Cu-rGO in multi scan rate.

Table 4.

CV of Cu-rGO specific capacitance value

S. NO	Area(10^{-5})	Charge(10^{-2})	Capacitance	Specific capacitance(F/g)
1	1.0256	0.0512	0.1025	68.37
2	1.2457	0.0622	0.1235	83.04
3	1.2651	0.0634	0.1268	84.54
4	1.6834	0.0841	0.1683	112.22
5	1.7457	0.0872	0.1745	116.38
6	1.8212	0.0910	0.1821	121.41
7	2.0602	0.1030	0.2060	137.35

result reveals that the redox potential behaviour of these nanoparticles was increased. From these above study it is clear that the Cu-rGO nanoparticles has highest sp in the multiscanning rate [20]. Cu-rGO nanoparticles of the scan rate are increase and the specific capacitance value will increase. The findings reported suggest that the developed sample will be evaluated as one of the acceptable electrode materials for energy storage devices in future attempts. rGO nanoparticles of the scan rate are increase and the specific capacitance value will decrease due to vacancy of carbon atom present in rGO.

Conclusion

The nanoparticles were made using a hydrothermal approach, and XRD, and TEM, EDX analyses were used to establish their crystalline size and morphological behaviour. The powder XRD data of rGO and Cu-rGO nanocomposites are used to estimate grain size, dislocation density, and micro strain. Cu-rGO nanoparticles are transparent in the visible and NIR areas, with a reduced cut-off wavelength of 233 nm, according to UV-Visible absorption spectra. The energy band (Eg) of rGO and Cu-rGO nanocomposites were found to be 1.5 and 2.31 eV, accordingly. The d-spacing value of Cu-rGO from XRD was well matched with d-spacing value of Cu-rGO of SEAD pattern. The specific capacitance values of r-GO and Cu-rGO calculated from CV in multi scan rate 68.37, 83.04, 84.54, 112.22, 116.38, 121,41 and 137.35(F/g) increased respectively. Comparative analyses of specific capacitance values show that Cu-rGO is a more appropriate material than rGO nanosheet for energy storage devices, batteries, and fuel cells. Cu nanoparticles have been embedded onto rGO nanosheets in TEM investigation, and SAED patterns identify a material's crystal structure, including its lattice characteristics. The fundamental groups were identified FTIR spectrum. All these studies indicate that the synthesized Cu-rGO nano particle can be considered as a potential candidate for the fabrication of batteries materials.

Shanmugam V. – Ph.D., Associate Professor department of physics;
Manimaran P. – Ph.D., Assistant Professor department of chemistry:
Seethalakshmi T. – Ph.D., Associate Professor department of physics.

[1] T. Jiao, H. Guo, Q. Zhang, et al., Reduced Graphene Oxide- Based Silver Nanoparticle-Containing Composite Hydrogel as Highly Efficient Dye Catalysts for Wastewater Treatment, Scientific Reports, 5(1), 11873 (2015); https://doi.org/10.1038/srep11873.
[2] M.Z.H Khan., *Graphene oxide modified electrodes for dopamine sensing*, Journal of Nanomaterials, 2017, vol. 2017, Article ID 8178314, 11 pages. https://doi.org/10.1155/2017/8178314.
[3] R. Ortega-Amaya, Y. Matsumoto, A.M. Espinoza-Rivas, M.A. Perez-Guzman, and M. Ortega-Lopez, *Development of highly faceted reduced graphene oxide-coated copper oxide and copper nanoparticles on a copper foil surface*, Beilstein Journal of Nanotechnology, 7, 1010 (2016); https://doi.org/10.3762/bjnano.7.93.
[4] W. Qi, P. Li, Y. Wu, et al., *Facile synthesis of $CoFe_2O_4$ nanoparticles anchored on graphene sheets for enhanced performance of lithium ion battery*, Progress in Natural Science: Materials International, 26(5), 498 (2016); https://doi.org/10.1016/j.pnsc.2016.09.001.
[5] H.H. El-Maghrabi, E.A. Nada, F.S. Soliman, Y.M. Moustafa, and A.E. Amin, *One pot environmental friendly nanocomposite synthesis of novel TiO_2-nanotubes on graphene sheets as effective photocatalyst*, Egyptian Journal of Petroleum, 25(4), 575 (2016); https://doi.org/10.1016/J.EJPE.2015.12.004.
[6] Seethalakshmi, Shanmugam, Vinitha, et al., *Graphite/MnO_2 Nanocomposites Assisted with PVA and PVP as Cathodic Active Materials,* International Journal of Scientific Research and Reviews, 7(3), 1600 (2018).
[7] D.R. Dreyer., S. Park, C.W. Bielawski, R.S. Ruoff, *The chemistry of graphene oxide*. Chem. Soc. Rev., 39, 228 (2010); https://doi.org/10.1039/B917103G.
[8] M. Hirata, T. Gotou, S. Horiuchi, M. Fujiwara, and M. Ohba, *Thin-film particles of graphite oxide 1: high-yield synthesis and flexibility of the particles*, Carbon, 42(14), 2929 (2004); https://doi.org/10.1016/j.carbon.2004.07.003.
[9] A. Furst, R.C. Berlo and S. Hooton, *Hydrazine as a reducing agent for organic compounds (catalytic hydrazine reductions)*, Chemical Reviews, 65(1), 51 (1965); https://doi.org/10.1021/cr60233a002.
[10] G. Wang, J. Yang, J. Park, et al., *Facile synthesis and characterization of graphene nanosheets*, 8e Journal of Physical Chemistry C, 112(22), 8192 (2008); https://doi.org/10.1021/jp710931h.
[11] M.B. Davies, J. Austin, and D.A. Partridge, *Vitamin C: Its Chemistry and Biochemistry*, Royal Society of Chemistry, London, UK, 1991.
[12] P. Manimaran and S. Balasubramaniyan, *Synthesis, Characterization and Biological Evaluation of Fe(III) and Cu(II) Complexes with 2,4-Dinitrophenyl hydrazine and Thiocyanate Ions*, Asian Journal of Chemistry; 31(4); 780 (2019); https://doi.org/10.14233/ajchem.2019.21719.
[13] D. Krishnan, F. Kim, J. Luo, R. Cruz-Silva, LJ. Cote, HD. Jang, J. Huang., *Energetic graphene oxide: Challenges and opportunities.* Nano Today, 7, 137 (2012); https://doi.org/10.1016/j.nantod.2012.02.003.
[14] V. Shanmugam S. Mohan M. Vishnudevan T. Seethalackshmi, M. Sathya, *Enhancement of specific capacitance and catalytic activities of MnO2 nanoparticles assist ed with PVA and PVP*, International journal of chem tech research, 11(05), 353 (2018); http://dx.doi.org/10.20902/IJCTR.2018.110539.

[15] G. Wang, J. Yang, J. Park, X. Gou, B. Wang, H. Liu, and J. Yao, *Facile Synthesis and Characterization of Graphene Nanosheets*. The Journal of Physical Chemistry C, 112, 8192 (2008); https://doi.org/10.1021/jp710931h.
[16] M. Nasrollahzadeh, F. Babaei, P. Fakhriand, and B. Jaleh, *Synthesis, Characterization, Structural, Optical Properties and Catalytic Activity of Reduced Graphene Oxide/ Copper Nanocomposites*, RSC Advance, 5, 10782(2015); https://doi.org/10.1039/C4RA12552E.
[17] S.T. Zhang, A.Y. Gu, H.F. Gao, and X.Q. Che, *Characterization of Exfoliated Graphite Prepared with the Method of Secondary Intervening*. International Journal of Industrial Chemistry, 2, 123 (2011).
[18] C. Fu, G. Zhao, H. Zhang, and S. Li, *Evaluation and Characterization of Reduced Graphene Oxide Nanosheets as Anode Materials for Lithium-Ion Batteries*. International Journal of Electrochemical Science, 8, 6269 (2013); https://doi.org/10.1016/S1452-3981(23)14760-2.
[19] Y. Zhu, S. Murali, W. Cai, X. Li, J.W. Suk, J.R. Potts, and R.S. Ruoff, *Graphene and Graphene Oxide. Synthesis, Properties, and Applications*. Advanced Materials, 22, 3906 (2010); https://doi.org/10.1002/adma.201001068.
[20] L. Shahriary, and A.A. Athawale, *Graphene Oxide Synthesized by Using Modified Hummers Approach*. International Journal of Renewable Energy and Environmental Engineering, 2, 58 (2014).

В. Шанмугам[1], П. Манімаран[2], Т. Сіталакшмі [1]

Питома ємнісна характеристика наночастинок Cu, вбудованих у нанопластини rGO, з використанням методу спільного осадження

[1]*Факультет фізики та досліджень, Урядовий коледж мистецтв (автономний), Карур, при університеті Бхаратідасан, Тіручіраппаллі, Тамілнад, Індія, nvsgacphy@gmail.com, seethabala@gmail.com;*
[2]*Факультет хімічних наук та досліджень, Урядовий коледж мистецтв (автономний), Карур, при Університеті Бхаратідасан, Тіручіраппаллі, Тамілнад, Індія*

Метод спільного осадження був використаний для синтезу наночастинок міді (Cu), закріплених на зменшеному оксиді графену (rGO). Результати PXRD, EDX і TEM підтвердили кристалічний розмір, функціональні групи та морфологічну структуру цих наночастинок. Дані порошкової рентгеноструктурної дифракції (XRD) для rGO і Cu-rGO нанокомпозитів були використані для оцінки розміру зерен, густини дислокацій та мікродеформацій. Згідно з УФ-спектрами поглинання, наночастинки Cu-rGO є непрозорими в оптичному та ближньому інфрачервоному діапазонах, із зниженою граничною довжиною хвилі 233 нм. Визначено, що ширина забороненої зони (Eg) для rGO і Cu-rGO становить відповідно 1,5 і 2,31 еВ. Значення міжплощинної відстані (d-spacing) для Cu-rGO, отримані за даними XRD та SEAD, виявилися дуже близькими. При використанні декількох швидкостей сканування питома ємність, розрахована з циклічної вольтамперометрії (CV), зростала як для rGO, так і для Cu-rGO.

Ключові слова: rGO, хімічне відновлення, композит Cu/rGO, циклічна вольтамперометрія.